Non-invasive measurement of retinal permeability in a diabetic rat model

Claire L Allen[1], Naseeb K Malhi[1], Jacqueline D Whatmore[2], David O Bates[1]*, Kenton P Arkill[1]*

[1] Division of Cancer and Stem Cells, School of Medicine, University of Nottingham Biodiscovery Institute, Science Road, University Park, NG7 2RD, United Kingdom.

[2] University of Exeter Medical School, St. Luke's Campus, Exeter, UK

*Authors contributed equally to the work

Correspondence

Dr Kenton P. Arkill and Professor David O. Bates

Division of Cancer and Stem Cells,

School of Medicine,

University of Nottingham Biodiscovery Institute,

Science Road,

University Park,

NG7 2RD,

United Kingdom.

Email: kenton.arkill@nottingham.ac.uk, david.bates@nottingham.ac.uk

Funding information

This work was supported by The Medical Research Council MR/P003214/1 (KA); and MR/L01985X/1 (DOB, JW); The National Eye Research Centre (DOB); and the Masonic Charitable Foundation (DOB).

Abstract

Objective: The gold standard for measuring blood-retinal barrier permeability is the Evans blue assay. However, this technique has limitations *in vivo,* including non-specific tissue binding and toxicity. This study describes a non-toxic, high throughput and cost effective alternative technique that minimizes animal usage. **Methods:** Sodium fluorescein fundus angiography was performed in non- and diabetic Brown Norway rats on days 0, 7, 14, 21 and 28. Sodium fluorescein intensity in the retinal interstitium and a main retinal vessel were measured over time. The intensity gradients were used to quantify retinal vascular permeability. Post study eyes were fixed, dissected and stained (isolectin B4) to measure required parameters for permeability quantification including: Total vessel length per retinal volume, radius and thickness. **Results:** In the non-diabetic cohort retinal permeability remained constant over the 28-day study period. However, in the diabetic cohort there was a significant and progressive increase in retinal permeability from day 14 to 28 ($p<0.01$, $p<0.001$, $p<0.0001$). **Conclusions**: This novel imaging methodology in combination with mathematical quantification allows retinal permeability to be non-invasively and accurately measured at multiple time points in the same animal. In addition, this technique is a non-toxic, rapid, sensitive and cost-effective alternative to the Evans blue assay.

Keywords: Retina; vessel; fundus fluorescein angiography; permeability; Fick's Law; quantitative; sensitive; non-toxic.

Abbreviations

EC	Endothelial cell

BBB	Blood-brain barrier
BRB	Blood-retinal barrier
EB	Evans blue
FFA	Fundus fluorescein angiography
STZ	Streptozotocin
i.p.	Intraperitoneal
GLUT2	Glucose transporter 2
Na-Fl	Sodium fluorescein salt
PBS	Phosphate buffered saline
avi	Audio video interleave
P_s	Solute permeability to solute *s* e.g. Fluorescein: $P_{fluorescein}$
OCT	Optical coherence tomography
RPE	Retinal pigmented epithelium
DR	Diabetic retinopathy

Introduction

Selective permeable barriers are vital for organ function and homeostasis. Such barriers include the EC barrier of blood vessels, the BBB[1], the BRB[2], the blood-spinal cord barrier[3] and the blood-placental barrier[4]. Selective transport of micromolecular substances across

these barriers occurs under physiological conditions but they are relatively impermeable to macromolecules such as albumin [5]. EB dye has a high affinity for albumin[6] and has a poor ability to cross selective permeable barriers under normal circumstances and remains predominantly within the blood circulation[5]. When diseases such as diabetic retinopathy[7], sepsis[8], capillary leak syndrome[9] or cancer[10] result in disruption of these barriers there is an increase in vascular permeability and dyes such as EB may extravasate from the circulation into surrounding tissues. Leak of dyes such as this across blood vessels or the BBB/BRB can signify damage and breakdown of the barrier via trauma or cytokine release. Accumulation of EB dye can be extracted from stained tissues and quantified by spectrophotometry[11, 12]. EB is extensively used to estimate changes in vascular permeability in a number of models including in stroke[13], cerebral ischaemia[11], skin[14] (often referred to as a Miles assay (Huang et al 2016), endothelial damage caused by trauma[15] and the breast cancer brain metastasis model[10]. EB has also been used to measure breakdown in the blood-spinal cord barrier[16] [17], and the BRB [18] [19].

The EB assay is rapid, sensitive and has become a widely used method for estimating barrier integrity and vascular permeability. However, this methodology has a number of significant assumptions associated with its use which can lead to significant over-simplification of the research findings if unaccounted for. These include: **(i)** the contribution of convective flux of albumin (and dye bound albumin) to the total flux varying from minimal to highly significantly dependent on haemodynamic parameters rather than barrier properties **(ii)** a substantive percent of free dye present in the animal following administration, resulting in flux being highly blood flow dependent rather than barrier dependent[1, 20] **(iii)** lack of specific binding to albumin, **(iv)** injection of dye dissolved in physiological solutions affects the structure of the dye, **(v)** EB binds albumin when it is in the tissues, (**vi**) change in tissue clearance can account for the changes **(vii)** problems with spectroscopic methods that have been used to estimate the amount of dye, and **(viii)** *in vivo* toxicity[20, 21]. These issues have been highlighted many times and are extensively discussed elsewhere.

This study describes a non-toxic and high throughput alternative technique to the EB assay in the retina. In combination with the Micron IV retinal imaging microscope system (Phoenix Research Systems, CA), we have used FFA and a novel post imaging analysis methodology described below. This technique can be carried out in less than 15 minutes, is minimally invasive and can be repeated in animals, resulting in a reduction of the number of animals required when compared to the EB assay, which takes 2-3 hours to carry out per animal and requires multiple cohorts of animals per time point. In addition, we have estimated that our novel methodology is significantly more efficient than the EB assay to perform.

Materials and Methods

Animals ethics: Experimental animals were treated in accordance with the ARVO Statement for the Use of Animals in Ophthalmic and Vision Research, and under a UK Home Office licence (PPL 30/3184), at the University of Nottingham Biological Services Unit.

Gender selection: Male Brown Norway rats, which are more susceptible to STZ-induced diabetes, (250-300g, Envigo, U.S.A) were included in this study.

STZ dose and route of administration: A total of 40 male Brown Norway rats were weighed and given a single intraperitoneal (i.p.) injection of STZ (Sigma–Aldrich, MO, U.S.A.). An additional 14 control rats were administered 300 µl saline i.p.

Fast or non-fasted prior to STZ dosing: Fasting can be used to minimize competition between STZ and glucose for low affinity GLUT2 transporters on β cells. In the period following STZ dosing the animals enter a hypoglycaemic state and begin to show signs of sudden weight loss, polyuria and dehydration. In our initial pilot study, animals were fasted overnight, prior to dosing in the morning, but their weights dropped dramatically during that period and this had a subsequent effect on weight loss in the proceeding study, exceeding a 20% weight loss moderate severity threshold. Therefore, in the subsequent study we did not fast prior to dosing. We ran the risk of the animals not becoming diabetic (~10% of cases) but this allowed the

animals to feed, retain or increase their weights prior to dosing and avoid the subsequent decline in health and weight otherwise observed. Animals with weights exceeding 300g tolerated the 50mg/kg STZ dose and maintained weights throughout the study or until the point of insulin supplementation.

Sucrose enrichment: In addition to water, a 15% (w/v) sucrose solution was made available in a separate drinking bottle to alleviate the initial hypoglycaemic spike following STZ induction. The volume of sucrose intake was monitored over a 72-hour period.

Insulin supplementation: Current blood glucose control in diabetic rodent models focuses on maintaining the diabetic animal in a state of moderate hyperglycaemia, with normal weight gain in the absence of severe ketonuria. This state can be achieved by once-daily injections of titrated insulin doses or by implantation of a continuous release insulin pellet. To reduce animal stress by repeated injections we subcutaneously implanted one third of a single insulin pellet (LinShin, Canada). The 7-mm long implant has a diameter of 2 mm and is designed to facilitate handling and insertion. Upon implantation, gradual erosion of the implant starts at once, and the effect of released insulin on the blood glucose level can be detected in <1h. Unlike injectable insulin, the implant releases a set basal dose of insulin every hour. Therefore, an animal given an optimal implant dose should show no glucosuria and ketonuria, which are both difficult to prevent by daily insulin injections, due to the action of the insulin lasting only part of the 24-hour cycle.

Blood glucose measurement: On days 0, 4 and prior to sacrifice (day 28) blood glucose levels were tested using a sample of blood taken from the tail vein and an Accuchek blood glucose monitor. Rats with blood glucose levels of >15 mmol/l and above were deemed hyperglycaemic. STZ-injected rats that did not become hyperglycaemic on day 4 were re-injected with STZ the following morning and subsequently evaluated for diabetes, as outlined above.

Optimisation of anaesthetic knockdown: Due to the severity of the diabetic model and in combination with injectable anaesthetics, gaseous anaesthesia (halothane) was trialled. However, this had constraints. Firstly, the small animal gaseous mask sat just underneath the eye making it very difficult to align the retinal microscope with the eye without dislodging the gaseous mask and risking the animal becoming lucid. Secondly, gaseous anaesthesia was not sufficient to prevent the eye from responding to the light source, blinking and rolling during imaging, without giving a high percentage of halothane. Injectable anaesthetic removed the cumbersome equipment required for gaseous knockdown, the control of multiple flow meters and ultimately stabilised the animal to prevent the eye from moving during FFA. We therefore used an injectable anaesthetic regimen combining ketamine hydrochloride, 37.5 mg/kg (Zoetis) and medetomidine hydrochloride, 0.25 mg/kg (Produlab Pharma BV) i.p.

Optimisation of Na-Fl dose and volume: Na-Fl (M.W. 376.27) was prepared in sterile water and 0.2μm filtered 0.1, 10, 100 mg/ml dilutions were prepared and stored at room temperature and away from direct light until required. Intraperitoneal injections were administered in a non-injected lower quadrant of the abdomen whilst the anaesthetised rat was on the imaging cradle and the retina of the right eye had been previously located and aligned using the Micron IV. This was achieved by raising the right back leg, maintaining retinal alignment by minimal animal movement. The retinal imaging software was set to record prior to injection and continued to record until the dye had reached a saturation level in the retina (~ 3 min).

Optimisation of Na-Fl route of administration: Two routes of administration, intraperitoneal and intravenous were tested with all three doses of Na-Fl. The tail was pre-warmed in a beaker of warm water (30-35 °C) to dilate the blood vessels and an intravenous injection was administered via the lateral tail vein. This method was more technically demanding and resulted in a sudden saturation of the retinal vasculature in approximately 30s. In comparison the i.p. route was simpler to administer and gave more gradual leakage of the dye into the retinal vasculature, over a period of approximately 3 min.

Animals were anaesthetised as previously described and transferred to an image cradle fitted with a heat mat. Viscotears was applied to the cornea of both eyes to prevent dehydration and whiskers were placed out of the field of view using a cotton tip. The Micron IV was advanced towards the cornea and the optic nerve was centred in the field of view, altering the brightness and focus to achieve a crisp image of the main retinal vessels. Once the eye was correctly aligned bright field fundus images of the retina were captured to check for any ocular abnormalities. The green filter was selected and a 3 min video footage of the retina was recorded at 15 frames per second. Animals then received a single 250 μl i.p. injection of Na-Fl. This was repeated on days 7, 14, 21 and 28 aligning the eye in the same position as captured on day 0. Development of cataracts with resultant blurring of posterior segment view meant that some eyes (n=2) were excluded from the consecutive FFA. Due to the rapid uptake and delayed elimination of Na-Fl from the animal's circulatory system only one eye could be imaged per session.

FFA analysis: Angiograms were imported as avi files into Fiji software[22] and mean fluorescence intensity was measured in a major retinal vessel and nearby tissue (which includes unresolved capillaries) every 200 frames up to 2400 frames. An initial time course was plotted and only the region where there was detectable tissue fluorescence but no major vessel saturation was used for analysis.

Immunofluorescence: Post euthanasia, on day 28, eyes were enucleated and immediately fixed in 4% PFA for 30 min. Retinae were excised from the scleral/choroidal cup and stained with an endothelial cell specific marker, isolectin B_4 (lectin from *Bandeiraea simplicifolia* conjugated to biotin) followed by Alexa Fluor 488-streptavidin. Whole-mounted retinae were imaged using confocal microscopy (Leica TCS SPE) to generate z stacks, and allow for analyses of vascular structural parameters across the superficial and deep plexuses. Length per volume and mean radius were measured using Fiji software[22] by manually drawing

along all vessels using the freehand line tool. The distance between the upper and lower plexus was taken as the vascular retinal thickness.

Statistical Analysis: Unless otherwise stated, all data are shown as mean±SEM. All data, and graphs were formulated with Microsoft Excel (Microsoft Office Software), GraphPad Prism v7/8 (GraphPad Software Inc., CA, U.S.A.), Fiji and Imaris. Vascular spacing statistical analysis was calculated using a one-way ANOVA with Bonferroni's correction and 28-day permeability analysis was calculated using a two-way ANOVA with Bonferroni's correction. All results were considered statistically significant at $p < 0.05$ (*), $p < 0.01$ (**), $p < 0.001$ (***), $p < 0.0001$ (****).

Results

To quantify the effective solute permeability (P_s) for the vascular wall the parameter derivation in Appendix 1 was used, which is directly comparable to previous derivations from single capillaries[23]. To enable this calculation to take place the fluorescence intensity was measured in one of the major retinal blood vessels, and in a box outside the major retinal vessel containing no visibly distinct vessels (i.e. no vessels larger than approximately 20μm in diameter, Figure 2A). The permeability to fluorescein ($P_{fluorescein}$) was estimated as described in Appendix 1 using FFA (Figure 2B). The calculations make the assumptions that the surface area available for exchange is the same in the diabetic animal as the control.

To determine these parameters tissue was stained to quantify the retinal vasculature. The retina has two clear plexuses (Figure 3A), one at the surface and one within the retinal layer. The vascular length (Figure 3B) and radius (Figure 3C) was calculated. There was no significant difference between the mean radius, the distance between the two plexuses (Figure 3D), nor the length of vessel per confocal volume.

We therefore calculated the permeability using cohort parameters and assuming that the surface area was unchanged throughout for each cohort. Figure 4A shows that while

permeability remained constant in non-diabetic animals, there was a significant and progressive increase in permeability in diabetic animals.

To determine whether permeability could be linked the data for all three diabetic and six controls over 28 days is shown (Figure 4B). These results show that the increase in permeability is progressive and that paired (linked) analysis can be used to determine a progressive increase in permeability with diabetic duration, allowing for a substantial reduction in number of animals per group as well as a reduction in overall numbers.

Discussion

These data show that the STZ model of diabetes (with insulin supplementation) in rats induces increased vascular permeability in the retina. This has been shown before via other methods [19] [18] and in other neuronal tissues, indicating a systemic response [19]. However, of note is that the permeability increases early including a trend at day 7, reaching significance by day 14, i.e. in early stages prior to gross vascular remodelling, as observed by measuring between the plexuses in the retina where there was no significant thickening (e.g. by oedema) of this layer. The FFA approach shown is practical, using repeated measures over a time course i.e. for therapeutic intervention, and could if desired be used in combination with other techniques such as OCT.

Leakage (increased solute flux from blood to tissue) can be caused by enhanced vascular permeability, increased driving force for flux (e.g. enhanced concentration gradient), increased surface area, or haemodynamic changes driving convective flux of solute. In the eye, homeostasis of the retina is maintained by the low permeability to proteins and water of the BRB. The outer BRB comprised of tight junctions between the RPE cells separates the choroid from the neuronal retina, and recent evidence indicates that it is also broken down in diabetes and contributes to retinal and macular oedema [19]. Evidence presented here confirms that the inner BRB, formed of the retinal vascular wall, becomes more permeable in this rat model of diabetes, contributing to the development of DR.

The current gold standard model of permeability measurement in the eye is the EB assay developed by Xu et al [18]. The EB assay can only be performed once per animal and therefore cannot be paired; hence, to be able to determine changes in permeability that develop over a four-week period, would require eight animals per group at three separate time points each (i.e. for three groups – control, diabetic, and diabetic+treatment) or a total of 72 animals. Eight animals per group are required because the measurements require the means of each group to be compared at each time point using a one-way analysis of variance, with post hoc analysis of each group resulting in 12 degrees of freedom (n=1 animals x n=1 groups = 6 x 2). In the methodology described here, the number per group can be reduced to a minimum of 3 because a two-way analysis of variance with a paired analysis is used resulting in the same 12 degrees of freedom (3 time points, n=1 groups, n=1 animals). This results in a reduction in numbers of animals to 9 in total. Thus, the current methodology could reduce the animal numbers required to determine whether an intervention reduces retinal permeability by 8-fold which can be inferred as an increase in methodological sensitivity.

The retina permits non-invasive and direct *in vivo* visualisation of neuronal tissue and vasculature. Retinal imaging is an important diagnostic tool in ophthalmic disease and changes in retinal vasculature are used to determine the severity of systemic disease. Imaging can be undertaken with and without contrast agents. Na-Fl has been given intravenously since the mid 1900s to temporarily highlight retinal vessels and thus improving *in vivo* assessment of the retinal circulation and BRB integrity [24, 25]. Currently Na-Fl is administered as a topical clinical tool for a host of conditions including diabetes[26], glaucoma[25], vascular occlusions[27], neovascularisation[28] and inflammatory disorders [29]. With the advancement in wide-field fluorescein angiography subtle changes in the peripheral BRB disruption can be detected [30]. The principal of FFA is a series of collated images over time to demonstrate choroidal, arterial and venous filling, and clearance. Images are then visually examined to identify non-perfused areas or retained fluorescence that may indicate vascular compromise as indicated by fluorescein leakage. However intermittent timing and inaccurate timing limits the analysis of fluorescein images to a qualitative assessment. Vascular

measurements that have been taken to date largely quantify the time it takes for Na-Fl to emerge in particular regions. Whilst useful, this does not provide information on the extent of change in the barrier function of the vasculature in any given location.

More recently, Hipwell *et al* have designed a method to analyse an entire fluorescein angiogram[31]. However, the analysis was limited to identifying the time to reach maximal fluorescence. Following on from this Hui *et al* and colleagues have outlined a quantitative spatial and temporal analysis of fluorescein angiography dynamics in a rodent model[32]. Therefore, the sensitivity is also limited to detect subtle changes such as differentiating vascular leakage from angiogenesis. However, video angiography could facilitate the quantitative analysis of more subtle differences in filling and leakage that occur in disease, for example early DR.

Permeability Quantification

Often permeability measurements determine solute flux, clearance or other parameters. When dealing with vasculopathies (e.g. diabetic) this can be important as individual exchange vessels can become more permeable, but the wider tissue could receive less molecules, for example due to fewer vessels. It is clear from EQ. 17 that the FFA technique is sensitive to the difference in the tissue and vessel intensity components; however, this is non-linear to the permeability so the ratio $< I_{V_1} > / < I_{V_2} >$ or derivatives can only be used phenomologically to determine true permeability changes (i.e. changes in the barrier function of the vessel wall). In this STZ rodent model of diabetes there were no significant differences for the vessel radius or exchange length but the result is sensitive to these parameters and our vascular assessment was not on the imaged volume but a similar area on the retina. We expect that if there was a wider understanding of the contextual vascular structure, particularly between animals, or we could use the specific vessels used to measure P_s, then it would tighten the point variation.

The P_s measured here is the effective P_s meaning that we have not taken into account capillary net pressure. The net pressure is the sum of the hydrostatic pressure out of, and the oncotic pressure into, the vessel. It is not currently possible to measure the pressure in the capillaries in the retina non-invasively, which can vary due to vascular shunting, local blood flow changes and global blood pressure. To do so would require sophisticated optical detection, and multiple fluorescent tracers: a large particulate tracer that can be imaged during flow, a large molecular weight molecule that cannot escape the vessels (or bright organic nanodots for example[33]), and a mid-sized molecule that can escape but not to the same extent as Na-Fl (353 Da in aqueous solution). Noting that this method is limited in the signal to noise in the measured tissue volume, brightness of the tracer will be an important practical factor without creating a sharp bolus (i.e. more invasive carotid injection). 10kDa (e.g. a chemokine) to 70kDa (e.g. albumin) molecules, if achieving a stable version bright enough to observe orders of magnitude lower fluxes, would be feasible sizes to test. Their flux fold-change would be measurable yet likely markedly different to Na-Fl itself and similar to water. The relative comparison may elude to which layers within the wall are disrupted in pathologies[34]. This would provide a better understanding of the flow dynamics and size selectivity but would still not be able to determine vascular hydrostatic or osmotic pressures. The change of ratio between the mid-sized and Na-Fl molecules would allow a more detailed understanding of the specific vascular wall layer that is disrupted in DR pathology.

Perspectives

In summary we highlight a simple, rapid, sensitive method for determining retinal permeability that can be used to drastically reduce the number of animals required to determine permeability changes in models of DR.

Acknowledgements

Appendix 1

From Fick's Law:

$$P_s = \frac{J_s}{S.\Delta C} \quad \text{EQ.1}$$

Where J_s is the flux of the number of molecules moving into the tissue (N_T)

$$J_s = \frac{dN_T}{dt} \quad \text{EQ.2}$$

S is the exchange area of the capillaries. ΔC = Difference in concentration between lumen C_V and tissue C_T but if we assume that initially C_T = 0 and throughout $C_T \ll C_V$:

$$\Delta C = C_V \quad \text{EQ.3}$$

If L_{Tot}= total length and r = mean radius of the vessels within the tissue imaging volume V_1 (see figure 2A) the exchange area (S) within V_1 becomes:

$$S = 2\pi r \mathrm{L}_{Tot} \quad \text{EQ.4}$$

V_1has a total number of molecules (N_{V_1}) being the sum of the molecules in the tissue (N_T) and capillaries (N_c) within it:

$$N_{V_1} = N_c + N_T \quad \text{EQ.5a}$$

$$N_T = N_{V_1} - N_c \quad \text{EQ.5b}$$

Hence:

$$\frac{dN_T}{dt} = \frac{dN_{V_1}}{dt} - \frac{dN_c}{dt} \quad \text{EQ.6}$$

When substituted in EQ.1 gives:

$$P_s = \frac{\left(\frac{dN_{V_1}}{dt} - \frac{dN_c}{dt}\right)}{S.C_V} \quad \text{EQ.7}$$

As all imaging volume V_2 is encompassed by the major vessel, the mean number of molecules in the unit volume is C_V.

$$\frac{N_{V_2}}{V_2} = C_V \quad \text{EQ.8}$$

$$< N_{V_2} >= C_V \quad \text{EQ.9}$$

Where < > denotes the mean over the respective volume. Further the number of molecules can be assumed to be directly proportional to fluorescent intensity (I) measured though-out (i.e. $I \propto \gamma N$) I therefore substitutes for γN to give:

$$P_s = \frac{\left(\frac{dI_{V_1}}{dt} - \frac{dI_c}{dt}\right)}{2\pi r \mathrm{L}_{Tot}.<I_{V_2}>} \quad \text{EQ.10}$$

If we assume the capillaries have the same solute concentration as the major vessel then:

$$I_c = \pi r^2 \mathrm{L}_{Tot} < I_{V_2} > \quad \text{EQ.11}$$

Subsequently:

$$\frac{dI_c}{dt} = \pi r^2 \mathrm{L}_{Tot} \frac{d<I_{V_2}>}{dt} \quad \text{EQ.12}$$

Substituting EQ.12 into EQ.10 gives:

$$P_s = \frac{dI_{V_1}}{dt} \cdot \frac{1}{2\pi r \mathrm{L}_{Tot} < I_{V_2} >} - \frac{r}{2 < I_{V_2} >} \cdot \frac{d < I_{V_2} >}{dt} \qquad \text{EQ.13}$$

The length of the vessels L_{con} in the confocal volume V_{con} (measured subsequent to euthanasia) contains all the vessel plexuses in the depth of field from the transport measurements, therefore:

$$\mathrm{L}_{Tot} = \frac{L_{con} V_1}{V_{con}} \qquad \text{EQ.14}$$

Substituting for L_{Tot} in EQ.13 gives:

$$P_s = \frac{V_{con}}{L_{con} V_1} \cdot \frac{dI_{V_1}}{dt} \cdot \frac{1}{2\pi r . < I_{V_2} >} - \frac{r}{2 < I_{V_2} >} \cdot \frac{d < I_{V_2} >}{dt} \qquad \text{EQ.15}$$

But:

$$\frac{1}{V_1} \cdot \frac{dI_{V_1}}{dt} = \frac{d < I_{V_1} >}{dt} \qquad \text{EQ.16}$$

So finally:

$$P_s = \frac{d < I_{V_1} >}{dt} \cdot \frac{V_{con}}{2\pi r . L_{con} . < I_{V_2} >} - \frac{r}{2 < I_{V_2} >} \cdot \frac{d < I_{V_2} >}{dt} \qquad \text{EQ.17}$$

One of the difficulties with these experiments is finding the real *t*=0. The tracer is via i.p. injection so takes time to reach the vasculature and travel via the heart and lungs to the retinal capillaries. Here $P_S^{t=0}$ is of the most interest as it fulfils the $\Delta C = C_V$ axiom. As in figure 2B to extrapolate to *t*=0 the $< I_{V_2} >$ and $< I_{V_1} >$ were plotted and *t*=0 defined as where the linear fit for each intercept. This was usually in the order of 20s different to frame timestamp. These linear fits were also used to calculate $P_S^{t=i}$ adjusting accordingly for the non-zero of the intensity intercept either from background or below the detection limit of the camera (this is not shown in Figure 2B). From $P_S^{t=i}$ an exponential fit (expected as C_T increases) was applied to determine $P_S^{t=0}$.

References

1. Kaya, M. and B. Ahishali, *The role of magnesium in edema and blood brain barrier disruption*, in *Magnesium in the Central Nervous System*, R. Vink and M. Nechifor, Editors. 2011: Adelaide (AU).
2. Cunha-Vaz, J., R. Bernardes, and C. Lobo, *Blood-retinal barrier.* Eur J Ophthalmol, 2011. **21 Suppl 6**: p. S3-9.
3. Bartanusz, V., et al., *The blood-spinal cord barrier: morphology and clinical implications.* Ann Neurol, 2011. **70**(2): p. 194-206.
4. Wang, Y., et al., *Endothelial barrier function in preeclampsia.* Front Biosci, 2007. **12**: p. 2412-24.
5. Kozler, P. and J. Pokorny, *Altered blood-brain barrier permeability and its effect on the distribution of Evans blue and sodium fluorescein in the rat brain applied by intracarotid injection.* Physiol Res, 2003. **52**(5): p. 607-14.
6. Wolman, M., et al., *Evaluation of the dye-protein tracers in pathophysiology of the blood-brain barrier.* Acta Neuropathol, 1981. **54**(1): p. 55-61.
7. Ved, N., et al., *Vascular endothelial growth factor-A165b ameliorates outer-retinal barrier and vascular dysfunction in the diabetic retina.* Clin Sci (Lond), 2017. **131**(12): p. 1225-1243.
8. Doi, K., et al., *Pre-existing renal disease promotes sepsis-induced acute kidney injury and worsens outcome.* Kidney Int, 2008. **74**(8): p. 1017-25.
9. Zhang, S., S. Wang, and S. Yao, *Evidence for development of capillary leak syndrome associated with cardiopulmonary bypass in pediatric patients with the homozygous C4A null phenotype.* Anesthesiology, 2004. **100**(6): p. 1387-93.
10. Do, J., et al., *Ex vivo Evans blue assessment of the blood brain barrier in three breast cancer brain metastasis models.* Breast Cancer Res Treat, 2014. **144**(1): p. 93-101.
11. Uyama, O., et al., *Quantitative evaluation of vascular permeability in the gerbil brain after transient ischemia using Evans blue fluorescence.* J Cereb Blood Flow Metab, 1988. **8**(2): p. 282-4.
12. Bates, D.O., *Vascular endothelial growth factors and vascular permeability.* Cardiovasc Res, 2010. **87**(2): p. 262-71.
13. Chen, B. and B.M. Fu, *An electrodiffusion-filtration model for effects of endothelial surface glycocalyx on microvessel permeability to macromolecules.* J Biomech Eng, 2004. **126**(5): p. 614-24.
14. Miles, A. and E. Miles, *Vascular reactions to histamine, histamine-liberator and leukotaxine in the skin of guinea pigs.* Journal of Physiology, 1952. **118**: p. 228-257.
15. Jackiewicz, T.A., et al., *Evans blue dye modifies the ultrastructure of normal and regenerating arterial endothelium in rats.* Microsurgery, 1998. **18**(1): p. 47-54.
16. Xu, J., et al., *Blockade of endogenous neurotrophic factors prevents the androgenic rescue of rat spinal motoneurons.* J Neurosci, 2001. **21**(12): p. 4366-72.
17. Ved, N., et al., *Diabetes-induced microvascular complications at the level of the spinal cord: a contributing factor in diabetic neuropathic pain.* J Physiol, 2018. **596**(16): p. 3675-3693.
18. Xu, Q., T. Qaum, and A. Adamis, *Sensitive blood-retinal barrier breakdown quantitation using Evans blue.* Invest Ophthalmol Vis Sci, 2001. **42**: p. 789-794.
19. Ved, N., et al., *Vascular endothelial growth factor-A165b ameliorates outer-retinal barrier and vascular dysfunction in the diabetic retina.* Clin Sci (Lond), 2017.

20. Moos, T. and K. Mollgard, *Cerebrovascular permeability to azo dyes and plasma proteins in rodents of different ages.* Neuropathol Appl Neurobiol, 1993. **19**(2): p. 120-7.
21. Hueper, W.C., *Reactions of the Blood and Organs of Dogs after Intravenous Injections of Solutions of Methyl Celluloses of Graded Molecular Weights.* Am J Pathol, 1944. **20**(4): p. 737-71.
22. Schindelin, J., et al., *Fiji: an open-source platform for biological-image analysis.* Nat Methods, 2012. **9**(7): p. 676-82.
23. Huxley, V.H., F.E. Curry, and R.H. Adamson, *Quantitative fluorescence microscopy on single capillaries: alpha-lactalbumin transport.* Am J Physiol, 1987. **252**(1 Pt 2): p. H188-97.
24. Novotny, H.R. and D.L. Alvis, *A method of photographing fluorescence in circulating blood in the human retina.* Circulation, 1961. **24**: p. 82-6.
25. Gass, J.D., et al., *A combined technique of fluorescein funduscopy and angiography of the eye.* Arch Ophthalmol, 1967. **78**(4): p. 455-61.
26. Vujosevic, S., et al., *Diabetic macular edema: fundus autofluorescence and functional correlations.* Invest Ophthalmol Vis Sci, 2011. **52**(1): p. 442-8.
27. Gong, H., Q. Song, and L. Wang, *Manifestations of central retinal artery occlusion revealed by fundus fluorescein angiography are associated with the degree of visual loss.* Exp Ther Med, 2016. **11**(6): p. 2420-2424.
28. Shah, S.M., et al., *Dynamic and quantitative analysis of choroidal neovascularization by fluorescein angiography.* Invest Ophthalmol Vis Sci, 2006. **47**(12): p. 5460-8.
29. Graham, E.M., et al., *Neovascularisation associated with posterior uveitis.* Br J Ophthalmol, 1987. **71**(11): p. 826-33.
30. Manivannan, A., et al., *Ultra-wide-field fluorescein angiography of the ocular fundus.* Am J Ophthalmol, 2005. **140**(3): p. 525-7.
31. Hipwell, J.H., et al., *Quantifying changes in retinal circulation: the generation of parametric images from fluorescein angiograms.* Physiol Meas, 1998. **19**(2): p. 165-80.
32. Hui, F., et al., *Quantitative spatial and temporal analysis of fluorescein angiography dynamics in the eye.* PLoS One, 2014. **9**(11): p. e111330.
33. O, M., *Brilliant organic nanodots: novel nano-objects for bionanophotonics.* SPIE Proc, 2008. **7040**: p. 704006-704017.
34. Owen-Woods, C., et al., *Local microvascular leakage promotes trafficking of activated neutrophils to remote organs.* J Clin Invest, 2020.

Figure legends

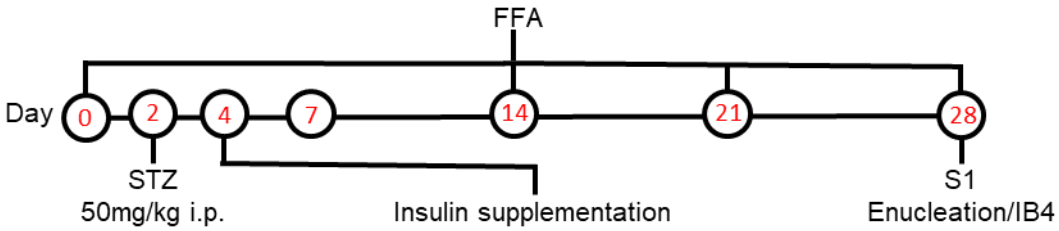

Figure 1. In vivo study overview and timeline. Male Brown Norway rats were given a single dose of STZ (50mg/kg) i.p. Non-diabetic controls were given an equivalent volume of sterile PBS i.p. On day 4 a tail vein blood sample was obtained and blood glucose levels measured. Diabetic animals were implanted with an insulin pellet and FFA was carried out on the left eye and in the same retinal position on days 0, 7, 14, 21 and 28. On day 28 animals were humanely killed by sacrifice and both eyes enucleated.

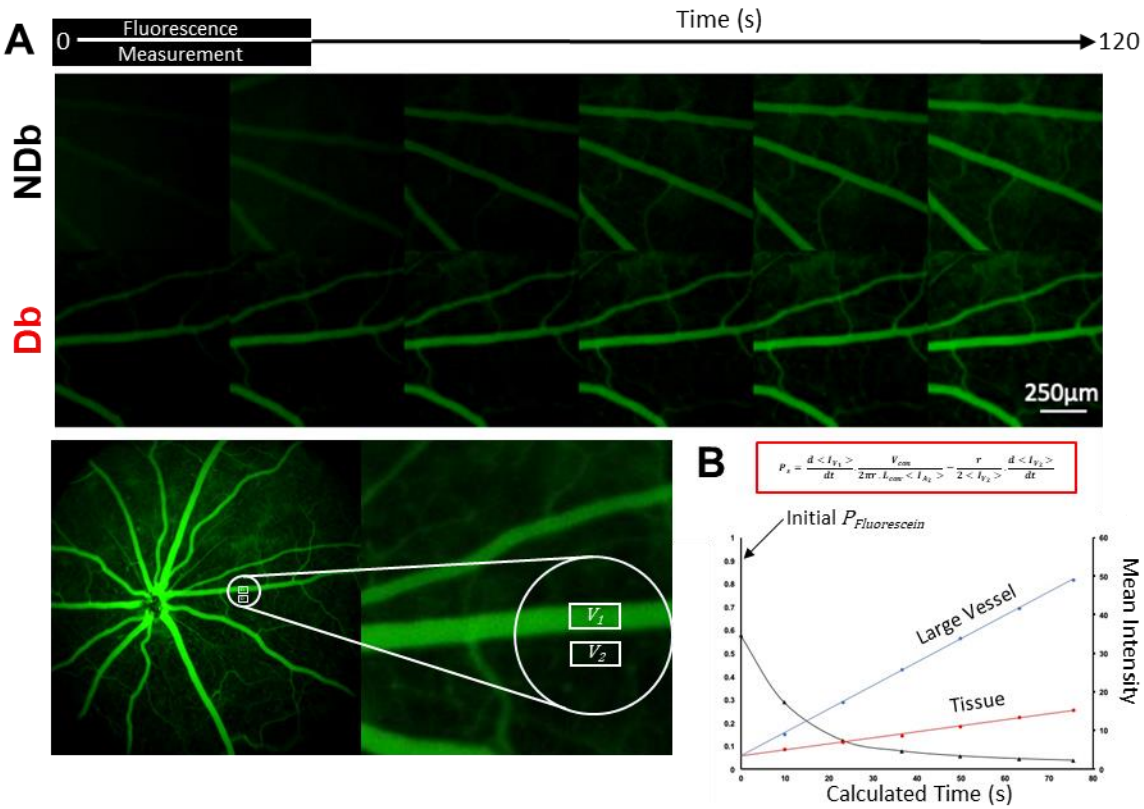

Figure 2. In vivo fundus fluorescein angiography methodology. Na-Fl FFA was performed in non- (NDb) and diabetic (Db) Brown Norway rats (250-300g) on days 0, 7, 14, 21 and 28. A 3-minute (15 fps) video was captured **(A)**. The mean intensity of Na-Fl in the retinal tissue ($< I_{V_1} >$) including unresolved capillaries and a main retinal vessel ($< I_{V_2} >$) were measured every 200 frames for 2 minutes. (**B**) Example of $< I_{V_1} >$ and $< I_{V_2} >$ over time used to determine initial fluorescein permeability ($P_{Fluoresein}^{t=0}$).

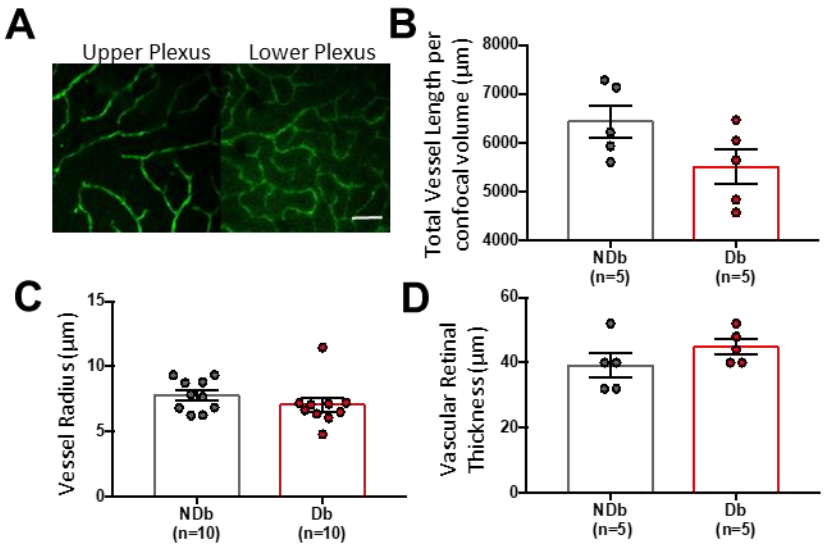

Figure 3. Retinal vessel dimensions remain unchanged in non-diabetic versus diabetic Brown Norway rats. Average retinal vessel length per confocal volume, radius and vascular retinal thickness were measured in non-diabetic (NDb) and diabetic (Db) cohorts prior to incorporating into the mathematical permeability equation. Eyes were enucleated at sacrifice, fixed, hemisected and retinae vessels stained (isolectin B_4). **(A)**. Total vessel length per confocal volume **(B)** and radius **(C)** measurements were calculated from non- and diabetic retina. **(D)** Vascular retinal thickness was measured from the upper to the lower plexus in the same animal cohorts. All data are shown as mean±SEM.

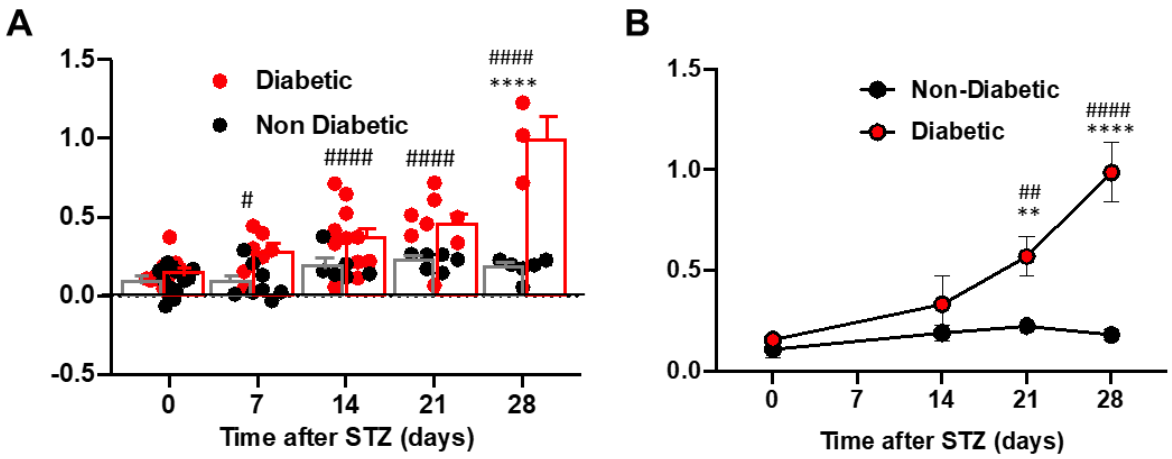

Figure 4. Retinal Na-Fl permeability $P^{t=0}_{Fluoresein}$ significantly increases over 28-days in diabetic Brown Norway rats and remains unchanged in non-diabetic controls. **(A)** Permeability measurements from 11 diabetic and 14 non-diabetic rats. Bars show mean±SEM. Paired one-way ANOVA, with Sidak post-hoc test. **(B)** Paired results from three diabetic and six non-diabetic rats followed for four time points. Statistical analysis using a two-way ANOVA, with Bonferroni's post-hoc test. $^{\#}p<0.05$ $^{\#\#}p<0.01$, $^{\#\#\#\#}p<0.0001$. $^{**}p<0.01$ and $^{****}p<0.0001$. $^{\#}$ denotes significance between time points, *denotes significance between non-diabetic vs diabetic per time point.